Research Square

Preprints are preliminary reports that have not undergone peer review.
They should not be considered conclusive, used to inform clinical practice,
or referenced by the media as validated information.

Rock Slope Stability and Water tightness Assessment of Arjo Didesa Dam site, Western Ethiopia

Legesse Asfaw
Addis Ababa Science and Technology University
Matebie Meten (matebe21@gmail.com)
Addis Ababa Science and Technology University, College of Applied Sciences, Department of Geology
https://orcid.org/0000-0002-1529-190X

Original Paper

Keywords: Arjo Didesa, Ethiopia, Leakage, Slope stability Water tightness

Posted Date: February 1st, 2021

DOI: https://doi.org/10.21203/rs.3.rs-190414/v1

License: This work is licensed under a Creative Commons Attribution 4.0 International License. Read Full License

Abstract

Arjo Didesa dam is an earth and rock fill dam which is under construction on the Didesa River in western Ethiopia. However, the dam encountered engineering geological problems that affected the water tightness and slope stability of the dam abutments and reservoir area. To solve these problems, different methods such as discontinuity survey, packer test, sampling and laboratory tests were applied to evaluate the engineering geological conditions of materials along the dam abutments and reservoir area on slope stability and water tightness. Slope stability analyses were performed by kinematic, limit equilibrium and finite element methods using laboratory and in-situ tests. Kinematic analyses revealed that both the left abutment slope 1(LAS1) and the right abutment slope 1(RAS1) sections were unstable for planar mode of failures. Further stability analyses using deterministic methods indicated that both sections were unstable only during saturated conditions. Similarly, stability analysis using limit equilibrium and finite element method revealed that both the left abutment slope 2(LAS2) and the right abutment slope 2(RAS2) sections were unstable under saturated conditions. This study also analyzed the permeability of soils and rock masses and the result showed that the permeability values range from $2.693*10^{-7}$cm/s – $6.687*10^{-5}$cm/s and $3.19*10^{-5}$cm/s – $1.3*10^{+1}$cm/s for soils and rock masses respectively. Integration of surface hydraulic conductivity and subsurface packer permeability tests showed the presence of potential leakage through the dam abutments. Remedial measures such as rock bolts, anchors and shotcrete for slope stabilization and grouting and clay blanketing are recommended to control this leakage.

1 Introduction

In a country like Ethiopia having with a great water resource, the construction of dams is very important for development. Both the federal and regional governments planned to construct large and micro dams in different part of the country including the Arjo Didesa Dam in order to improve food security. However, most of the dam constructed on volcanic and sedimentary terrains in different parts of the country have faced engineering geological problems such as leakage, reservoir siltation, slope instability, damages of spillway and dam body without giving their desired purposes (Haregeweyn et al. 2006; Abdulkadir 2009; and Berhane et al. 2013). Nowadays, leakage of water is a common problem almost in all the dam sites in the world (Mozafari et al. 2011). Leakage problem may lead to water losses from the reservoir and slope instability problem of the dam body and dam abutments. These water losses could occur through the dam body, dam foundation and dam abutments. Moreover, geological structures such as joints and faults are causing excessive leakage of water from the reservoir which leads to failure of the dam (Fell et al. 2005). This scenario was, even more, bigger for the dam constructed in highly weathered and fractured volcanic rocks as in the current study area.

Similarly, slope failure is one of the hazards that lead to the damage of different engineering structures such as dams, tunnels and roads. Slope instability may occur due to the factors such as geological defects, adverse slope geometries, high degree of weathering of slope materials, human activity, heavy precipitation and seismicity which can significantly destabilize slopes (Basahel and Mitri 2018). From this perspective, considering the stability of the abutments of a dam is very essential as numerous dams all over the world encountered abutment slope stability problems. Vaiont dam failure, which occurred in Italy in 1963, was a typical example of dam abutment failures due to sliding of rock abutments. As a result of this a huge mass of rock blocks slided into the reservoir which generated a wave overtopping the dam and took about 2500 lives (Genevois and Ghirotti 2005). Sliding of a 5 million m^3 mass into the reservoir of the Pontesei Dam reduced the basin capacity by about 50% (Panizzo et al. 2005). After the first impoundment of the Three Gorges Dam, a reservoir landslide occurred due to the movement on bedding-plane shears (Wang et al. 2004). In a routinely monitored and inspected Clyde Dam, several large landslides have also occurred along the reservoir margins prior to impoundment (Macfarlane 2009). Slope stability analysis has a long history in geotechnical engineering and engineering geology and recently it is one of the most active areas in both practice and research to prevent this natural disaster (Hussain et al. 2019). Currently, a number of methods are being used for slope stability assessment such as kinematic, limit equilibrium (LE) and finite element (FE) methods that are widely used by many researchers (Raghuvanshi 2017 and Shaz et al. 2019).

Kinematic analysis is useful to investigate the possible mode of failure of rock masses without determining the factor of safety (Gischig et al. 2011), while the LE and FE methods analyze the stability of the slopes in terms of factor of safety(FOS) (Kanungo et al. 2013). Besides, in the limit equilibrium method, the factor of safety were calculated for pre-determined failure surfaces which divided into a number of slices based on the force and moment equilibrium (Kanungo et al. 2013). However, for FE method doesn't require the shape and location of the failure slip surface (Griffiths and Lane 1999). The FE method preserves global equilibrium until failure is reached and can monitor progressive failure up to and including the overall shear failure (Vinod et al. 2017). Moreover, FEM is the most suitable methods for blocky to very blocky rock mass as its results represents the actual field conditions (Pain et al. 2014).

The present study is aimed to investigate the engineering geological problems of the Arjo Didesa dam site which is under construction on Didesa River in the volcanic terrain of Southwestern Ethiopian plateau (Fig. 1). However, the dam has encountered engineering geological problems like slope instability and water tightness of the dam abutments and reservoir area respectively. The presence of open joints in dam abutments that is filled by secondary fine materials can possibly trigger the lubrication of materials when impounded water moves along the fracture beneath the reservoir. This will lead to a potential leakage of water from the reservoir as the orientation of joints may favorable this phenomenon. Thus, in order to understand and solve these water tightness and slope instability problems different methods were followed such as geological and engineering geological mapping, discontinuity surveying, packer permeability test, sampling and laboratory testing which helped to evaluate the conditions of materials along the dam abutments and reservoir area. For slope stability analyses of the dam abutments, kinematic, deterministic and numerical modeling methods were applied.

1.1 Geology and Tectonic Setting

In the southwestern Ethiopian plateau, the exposed geological units dominantly consist of the Precambrian basement rocks and associated intrusive rock, Paleozoic sediments, Mesozoic sediments, Tertiary volcanic and quaternary deposits (Tefera et al. 1996 and Alen and Taddesse 2003). The study area is geologically characterized by the presences of Precambrian rocks/basement complex which covers the NW and Central part of Arjo area (Merla et al. 1973) while the Paleozoic-Mesozoic sedimentary rocks and Cenozoic rocks consist of Tertiary volcanic and quaternary superficial deposits that comprised of continental clastic sediments of Getema and Wama Sandstones covering the NE and SE part of Arjo area (Alemu 2014, unpublished research work) and the Tertiary volcanic rocks covered large parts of the area including Dam site that represents Jima Volcanics and Wollega basalt (Merla et al. 1973). The geological structures and tectonic setting of the southwestern Ethiopian Plateau are characterized by the presence of lineaments and faults (Alen and Taddesse 2003). The lineaments of the study area have four general directional trends i.e. (i) N-S (ii) NNE-SSW to NE-SW (iii) NW-SE to WNW-ESE and (iv) ENE-WSW directions while faults of area are represented by high-angle normal faults, low-angle normal slip faults and strike-slip faults (Alemu 2014, unpublished research work).

2 Methods

In this study, engineering geological assessments were carried out through detail fieldwork and laboratory analysis to determine the index and engineering properties of soils and rocks that constitute at the dam site and within reservoir area. The fieldwork included discontinuity surveying, mapping, digging test pits, in-situ strength and packer permeability test and sampling. Discontinuity survey includes describing discontinuity orientation, spacing, roughness, persistence, aperture and filling material based on the standard suggested by ISRM (1981). Discontinuity data were used to determine the hydraulic conductivity of the surface rock masses and for slope stability analysis. The laboratory test on the soil samples include natural moisture content, specific gravity, particle size analysis, liquid limit test and permeability tests while the laboratory tests conducted on rock samples are point load and unit weight tests. Besides, the in-situ strength of rocks was also determined using the Schmidt hammer on selected slope sections according to the standard suggested by ASTM

(2001). Accordingly, the point load (Broch and Franklin 1972) and in-situ strength Schmidt hammer test (Aydin 2009) were used to determine the uniaxial compressive strength of intact rocks. Rock Quality Designation (RQD) and Geological Strength Index (GSI) assessments were also carried out in the fieldwork to determine the quality of rocks at dam site. GSI was estimated based on basic GSI charts proposed by Marinos and Hoek (2000) whereas the RQD has been estimated from joint volumetric count (JV) as follows using eq. 1 as suggested by Palmstrom (1982).

RQD = 115 – 3.3Jv …….(1)

Furthermore, slope stability analyses of the dam abutments were conducted using the Kinematic, limit equilibrium and finite element methods. The kinematic analyses were performed using Dips 6 software (Rocscience 2004) for the structural controlled slope sections i.e. left abutment slope 1(LAS1) and right abutment slope 1(RAS1) sections which are lying on the left and right abutments respectively (Fig. 2) and further stability analysis for these particular slope sections was carried out in terms of factor of safety (FOS) by deterministic method using RocPlane software (Rocscience 2004). Similarly, stability analysis of highly weathered and fractured (non-structurally controlled) slope sections i.e. left abutment slope 2(LAS2) and right abutment 2(RAS2) slope sections (Fig. 2) was done by limit equilibrium method (LEM) and finite element method (FEM) using Slide v6.0 (Rocscience 2004) and Phase 2 v8.0 software respectively in terms of FOS.

Moreover, water tightness analysis was performed through laboratory permeability tests on soils, packer permeability tests and hydraulic conductivity estimation from the aperture and spacing of fractures from the surface of rock mass using eq. 2 of Snow (1965) and Louis (1974) by assuming that the fractures are parallel and smooth.

$$K = \frac{\lambda g e^3}{12\mu} \quad \ldots\ldots(2)$$

Where g is the gravitational acceleration (9.81m/s^2), e is the average aperture of fractures (m), μ is the coefficient of kinematic viscosity of the fluid (10^{-6}m^2/s for water at 20□c) and λ is the fracture frequency. The general methodological framework of the study is shown in Fig. 2 as follows.

3 Result And Discussion

3.1 Geology of the Study Area

The lithological units in the study area consist of rhyolite, basalt, alluvial soil, residual soil and colluvium deposit (Fig. 3). The rhyolite rock is exposed at dam abutments and in the reservoir area which is characterized by high degree of weathering and fracturing and porphyritic in texture. In this rock unit, the joints were partially filled with fine soils and soft gouge. The basaltic rock is the dominant rocks in the study area which is characterized by different degree of weathering from highly to slightly weathered and aphanitic in textures, dark to grey in color. The colluvial deposit is deposited under gravity force along the dam abutment slopes. It is a mixture of an extremely wide range of soil types which ranges from fine to coarse-grained soils. These materials are likely to be highly permeable. Furthermore, the reservoir area is dominantly covered by alluvial and residual soils. Alluvial and residual soils are covering a large part of Didesa plain which is part of the reservoir area and is characterized by mixtures of major soil types from silty clay to coarse sands and gravels. As observed from in-situ test pits and drilled boreholes along the dam axis, the thickness of this soil ranges from 2 to 5m.

3.2 Discontinuity Surveying

The discontinuity survey analysis revealed that majority of the joint sets were having larger continuity, vertical to sub-vertical orientation and the aperture and spacing of discontinuity varied from 0.1cm to 0.7cm and 1-120cm respectively (Table 1). They are characterized by slightly rough to smooth discontinuities and moderately to highly weathered ones as per ISRM (1981) (Table 1). Majority of the joints have favorable orientation for leakage as these discontinuities crossed the dam axis nearly parallel to the direction of river flow. As shown in Fig. 4 in the left abutment, JS1 has a very favorable orientation for leakage whereas in the right abutment, JS3 has a very favorable orientation for leakage as these are oriented parallel to the direction of river flow. Therefore, these conditions will lead to a potential leakage of water from the reservoir area. Hence, special treatment is required at the dam abutments during the construction stage in order to control this leakage.

3.3 Rock mass Classification

In the present study the two most widely used rock mass classification methods, namely rock mass rating(RMR) (Bieniawski, 1989) and geological strength index(GSI) (Marinos and Hoek, 2000) have been used to characterize the rock mass and estimate the rock mass quality at the left and right abutments of the dam. The RMR system consists of five basic parameters that represent different conditions of rock mass and discontinuities (Table 1). Based on RMR, the rock mass quality falls in the range of poor to good quality rocks with RMR values ranging from 33 to 63 (Table 1) while in the case of GSI, the rock mass quality was classified in the range of disintegrated to very blocky with GSI values ranging from 15 to 65 as estimated in the field (Table 2).

Table 1 RMR values and classification of rocks at the dam site based on Bieniawski (1989)

Location		Left Abutment				Right Abutment			
		Observation Slope Sections							
		LAS1		LAS2		RAS1		RAS2	
Discontinuity Parameters		Condition	Ra	Condition	Ra	Condition	Ra	Condition	Ra
UCS (MPa) [a]		48.97	4	24.24	2	39.13	4	23.3	2
RQD (%) [a]		52.35	13	23.49	3	69.31	13	42.98	8
Spacing(cm)		1 – 120	15	5 – 40	5	5 – 115	15	1– 85	5
Discontinuity Condition	Aperture(cm)	0.1– 0.15	1	0.02 – 10	0	0.3 - 10	0	0.1- 1	0
	Persistence(m)	1.5 – 3	4	0.5 – 1.3	4	1.5 - 5	2	0.4- 1.6	4
	Roughness	Rough	5	S. Rough	3	S. Rough	3	S. Rough	3
	Filling	Soft Gouge	0	Fine material	0	Clean	6	Fine material	2
	Weathering Degree	Moderately Weathered	3	Highly Weathered	1	Slightly weathered	5	Highly weathered	1
Groundwater cond.		Dry	15	Damp	15	Dry	15	Dry	15
RMR rating values		60		33		63		40	
Class		III		IV		II		III	
Description		Fair rock		Poor Rock		Good rock		poor rock	
Where; Ra is Rating value, [a] is an average value, S is Slightly									

Table 2 GSI values at the left and right abutments of the dam

Location	Slope Sections	GSI values determined from RMR_{89}	GSI range field estimation	Rock units
Left Abutment	LAS1	55	45-60 (53)[a]	Slightly weathered Rhyolite
	LAS2	28	15-30 (23)[a]	Moderately weathered Rhyolite
			15-20(18) [a]	Highly weathered Rhyolite
Right Abutment	RAS1	58	50-65 (58) [a]	Slightly weathered Rhyolite
	RAS2	35	25-30 (28) [a]	Highly weathered Rhyolite
			30-40(35) [a]	Moderately to Slightly weathered Rhyolite
Where GSI = Geological Strength Index, [a] = Average value				

3.4 Rock Mass Strength and Deformation parameters

In this study RocLab software (Rocscience 2002) was used to determine the geomechanical properties of the rock mass for non-structurally controlled slope sections. The input parameters used in RocLab software were given in Table 3. The GSI values determined in the field (Table 2) and disturbance factor(D) values taken from (Torres and Brent 2002) were used in the slope stability analysis. Similarly, the material constant of the intact rock (mi) was also taken from (Rocsience 2002) and for rhyolite rock, the value of mi is considered to be 25. The Young's modulus(Erm) was determined using eq. 4 (Hoek and Diederichs 2006). For isotropic rocks, in some rock engineering applications with limited field data, a value between 0.2 and 0.3 is a common estimate for Poisson's ratio (Gercek 2007). Thus, for this study its value was assumed to be 0.3. The intact modulus (E_i) was determined using eq. 3 and the modulus ratio (MR) value of the rhyolite rock was assumed to be 400 as proposed by Deere (1968). This relationship is useful when measurement of Ei is difficult for completely undisturbed rock samples. The estimated geo-mechanical properties of the rock masses were presented in Table 4.

$$E_i = MR\sigma ci \quad (3)$$

$$Erm = E_i * (0.02 + \frac{1-D/2}{1+e(\frac{60+15D-GSI}{11})}) \quad (4)$$

Table 3 Input parameters used in RocLab software

Slope Sections	Rock units	Input Parameters for RocLab					
		σci(MPa)	GSI	mi	D	γ(MN/m^3)	H(m)
LAS2	Highly weathered Rhyolite	23.46	18	25	0.7	0.02184	80
	Moderately weathered Rhyolite	25.3	23	25	0.7	0.02489	80
RAS2	Highly weathered Rhyolite	20.77	28	25	0.7	0.02184	85
	Moderately to Slightly weathered Rhyolite	25.9	35	25	0.7	0.02489	85
Where σci is the uniaxial compressive strength of intact rock, mi is rock material constant, γ is unit weight and H is slope height							

Table 4 Geo-mechanical properties of the rock mass

Slope Section		**Output Parameters of RocLab**						
		Mohr-Columb Fit		Hoek-Brown Constant			Erm(kPa)	v
		C(MPa)	□(□)	Mb	S	a		
LAS2	HWR	0.162	25.96	0.276	6.9e-6	0.55	238000	0.3
	MWR	0.223	28.56	0.364	1.42e-5	0.536	288900	0.3
RAS2	HWR	0.226	30.84	0.478	2.94e-5	0.526	276900	0.3
	SWR	0.339	34.66	0.703	8.106e-5	0.516	464100	0.3
Where C is Cohesion, □ is Friction angle, mb, s, and a are rock mass material constants, Erm is the modulus of elasticity, v is Poisson's ratio and HWR, MWR and SWR represent highly weathered rhyolite, moderately weathered rhyolite and slightly weathered rhyolite respectively.								

Similarly, for structurally controlled slope sections, the shear strength parameters of the rock mass along the discontinuity failure planes were determined from RocData software (Rocscience, 2004) (Table 5). The joint wall compressive strength (JCS) corresponding to 25% of uniaxial compressive strength of intact rock was determined from Schmidt hammer tests whereas the joint roughness profile (JRC) value was determined visually in the fieldwork by comparing the appearance of the discontinuity surface with the standard developed by Barton and Choubey (1977). The values of the basic friction angle (ϕ_b) for most of the smooth and unweathered rock surfaces range between 25^0 and 35^0 (Barton, 1973). Hence in this study, the basic friction angle of 30^0 was considered.

Table 5 Shear strength parameters along the potential joint planes that caused failures at critical slope sections

Slope sections	Potential Joint Plane	Input parameters of RocData software for Barton-Bandis failure criteria					The output result of RocData software	
		JCS(MPa)	JRC	$\phi b(^0)$	$\gamma(MN/m^3)$	H(m)	$\phi(^0)$	C(MPa)
LAS1	J2	14.17	5	30	0.02337	30	35.40	0.020
	J3	32.15	4	30	0.02337	35	35.52	0.018
RAS1	J3	39.88	5	30	0.02337	26	37.87	0.019

4 Slope Stability Analysis Results

4.1 Kinematic Analysis

Discontinuity and slope orientation that were used in the Dips software for kinematic analysis were measured in the field (Table 6) whereas the friction angle along the failure plane was estimated in RocData software (Table 6). The kinematic analyses revealed that planar mode of failure occurred due to the intersection of joint set 2 (JS2) and Joint set 3 (JS3) at LAS1 (Fig. 5a) while at RAS1, planar mode of failure occurred due to joint set 3 (JS3) (Fig. 5b).

Table 6
Input parameters used in Dips software for kinematic analysis

Slope sections	**Slope orientation of slope**	**The orientation of discontinuity (Dip/ Dip direction) (°)**			**Friction angle**	**Output Possible mode of failure**
	(dip/dip direction(°))	**J1**	**J2**	**J3**		
LAS1	65/068SE	55/250	45/106	42/020	35	Planar failures (J2 and J3)
RAS1	56/230SW	46/090	38/290	45/210	38	Planar failures (J3)

4.2 Stability Analysis using Deterministic Method

The stability analysis for the planar mode of failure was performed by deterministic method using RocPlane software (Rocscience 2002) in terms of FOS (Park and West 2001). The input parameters used in RocPlane software were given in Table 7. The horizontal seismic acceleration of the study area from Johnson and Degraff (1991) was estimated to be 0.01g. This was used in this analysis.

Table 7
Input parameters used in RocPlane software

Slope sections	Potential Joint Plane	Geometry						shear strength		Forces	
		Slope angle	Upper slope angle	Failure plane angle	Slope Height	γ (t/m^3)	W	⍰ (^{0})	C(t/m^2)	u_w (t/m^3)	α(g)
LAS1	J2	65	15	45	30	2.337	8	35.40	2.0	1	0.01
	J3	65	12	42	35	2.337	4	35.52	1.8	1	0.01
RAS1	J3	56	12	40	26	2.337	5	37.87	1.9	1	0.01
Where γ is the unit weight of the rock, w is waviness, ⍰ is friction angle, c is cohesion, u_w is water pressure, α is the seismic coefficient											

FOS was calculated under different anticipated conditions i.e. static condition(without earthquake loading) and dynamic condition(with earthquake loading) by varying water pressure level, percent filled in the joints i.e. dry condition when 0% is filled, a moderate condition when 50% is filled and fully saturated condition when 100% is filled (Table 8). The analysis result revealed that at both LAS1 and RAS1 slope sections, the FOS is less than one only during saturated conditions (Table 8) and the slope was found to be unstable (Wyllie and Norrish 1996) (Fig. 6). This indicated that pore water pressure significantly contributed to destabilize these particular slope sections as compared to seismic activity as the study area falls in low seismic risk zone (Asfaw 1986). In addition, the field the geometry of the slopes and orientation of discontinuity also played a greater role in destabilizing these particular slope sections.

Table 8
Factor of safety determined for planar mode of failures in different conditions

Slope section	Potential failure plane	FOS					
		Static condition			Dynamic condition		
		Dry	Moderately	Fully saturated	Dry	Moderately	Fully saturated
LAS1	J2	1.07	0.86	0.25	1.05	0.84	0.24
	J3	1.02	0.85	0.34	1.0	0.83	0.33
RAS1	J3	1.32	1.08	0.33	1.30	1.05	0.32

4.3 Stability Analysis by LEM

LE and FE method is the most suitable for the analysis of highly weathered and fractured slope materials (Mahboubi et al. 2008). Hence, the slope stability analysis of highly weathered and fractured slope sections of the left abutment slope 2(LAS2) and right abutment slope 2(RAS2) were carried out using LE and FE methods in terms of Factor of Safety. The LE methods are based on force and moment equilibrium while the FE methods use the stress-strain relationships to determine the behavior of the model (Memon 2018). Slope stability analysis using LEM was performed using GLE/Morgenstern-Price/ method using Slide v6.0 software (Fig. 7). Hence, FOS was calculated under different anticipated conditions i.e. before impoundment of water in the reservoir (dry condition) and after impoundment of water in the reservoir (saturated condition) under both static and dynamic conditions (Table 10). The input parameters used in slide

software were given in Table 9. The shear strength parameters (cohesion and friction angle) of rocks that were used in the analysis were given in Table 5 whereas the geometry of the slope was measured in the field.

Table 9
Input parameters used slide software

Material	Parameters			Slope Geometry		α(g)
	C (MPa)	ϕ (°)	γ (KN/m^3)	Height (m)	Angle (°)	
Left Abutment Slope 2 (LAS2)						
Layer 1(HWR)	0.162	25.96	21.84	80	54	0.01
Layer 2(MWR)	0.223	28.56	24.89	80	54	0.01
Right Abutment Slope 2 (RAS2)						
Layer 1(HWR)	0.226	30.84	21.84	85	47	0.01
Layer 2(SWR)	0.339	34.66	24.89	85	47	0.01
Where C is Cohesion, ϕ is Friction angle, γ is the unit weight of the rock, α is Horizontal seismic acceleration and HWR, MWR and SWR represent highly weathered rhyolite, moderately weathered rhyolite and slightly weathered rhyolite respectively.						

The analysis results revealed that at both LAS2 and RAS2 slope sections, the FOS is less than one and the slope was found to be unstable during saturated conditions and stable under dry conditions (Table 10) (Wyllie and Norrish 1996). This indicated that the pore water pressure significantly contributed to the instability of these particular slope sections as compared to horizontal seismic acceleration. The other factor affecting the stability of these slope sections was the geometry of the slopes that needs to reduce the angle of these slopes for a better slope stability.

Table 10
Stability analysis results by LEM utilizing GLE/Morgenstern-Price/Method

Conditions	The factor of safety (FOS)			
	Static		Dynamic	
	Dry condition	Saturated condition	Dry condition	Saturated condition
Left Abutment Slope 2 (LAS2)				
Factor of Safety (FOS)	1.099	0.377	1.088	0.367
Resisting Horizontal Force(KN)	1109.95	212.758	1104.91	210.707
Driving Horizontal Force(KN)	1009.97	564.653	1015.35	574.095
Resisting moment (KN/m)	177298	15529.6	176578	15202.9
Driving moment (KN/m)	161327	41214.9	162264	41422.2
Right Abutment Slope 2 (RAS2)				
Factor of Safety (FOS)	1.499	0.683	1.474	0.132
Resisting Horizontal Force(KN)	3452.58	789.473	3424.58	6.255
Driving Horizontal Force(KN)	2303.67	1155.55	2322.81	47.516
Resisting moment (KN/m)	440870	110378	436672	832.497
Driving moment (KN/m)	294162	161561	296185	6323.57

4.4 Slope Stability Analysis by FEM

Slope stability analysis of LAS2 and RAS2 slope sections were further evaluated using the finite element method (FEM) in terms of the critical strength reduction factor (SRF) to confirm the stability conditions of these slope sections. Hence, the critical SRF was calculated using Pahse2 V8.0 software under different anticipated conditions (Figs. 8 and 9). The shear strength reduction option in Phase2 software was used to perform a finite element slope stability analysis and compute a critical SRF. The input parameters used in Phase2 were given in Table 11.

Table 11
Input parameters for Phase2 software

Rock units	Parameters					Slope Geometry		α (g)
	C (MPa)	ϕ (°)	γ (KN/m^3)	Erm (MPa)	V	Height (m)	Angle (°)	
Left Abutment Slope 2 (LAS2)								
Layer 1(HWR)	0.162	25.96	21.84	238	0.3	80	54	0.01
Layer 2(MWR)	0.223	28.56	24.89	288.9	0.3	80	54	0.01
Right Abutment Slope 2 (RAS2)								
Layer 1(HWR)	0.235	30.84	21.84	276.9	0.3	85	47	0.01
Layer 2(SWR)	0.339	34.66	24.89	464.1	0.3	85	47	0.01
Where C is Cohesion, ϕ is Friction angle, γ is the unit weight of the rock, α is Horizontal seismic acceleration and HWR, MWR and SWR represent highly weathered rhyolite, moderately weathered rhyolite, and slightly weathered rhyolite respectively.								

The analyses result revealed that when both slope sections are at static and dynamic saturated conditions, the critical SRF is less than one and the slopes were unstable while when the slopes are in dry conditions, the critical SRF was greater than one and the slope was stable according to Wyllie and Norrish (1996) (Figs. 8 and 9). This showed that the effect of water pressure plays a greater role in destabilizing these particular slope sections as compared to horizontal seismic acceleration.

When the results of the FE analyses were compared with the result obtained from the LE method, the FOS results determined from the FEM were in very good agreement with those computed by the LEM (Fig. 10). Furthermore, slip failure surfaces were almost the same for both techniques. Besides, the analyses results revealed that the slope sections of the left and right abutments of the dam are unstable only during saturated conditions. Several researchers have previously compared the results of slope stability analyses using the LE and FE methods (Cheng et al. 2007 and Vinod et al. 2017). They concluded that the results of both methods were generally in a good agreement for homogenous slopes. But, the FE method is more advanced and valuable than the LE method in case of slope modeling and design with heterogeneous materials, complex slope geometry and different loading patterns. In general, the present study concluded that the results of both FE and LE methods were in good agreement under different anticipated conditions when simple slope geometry and heterogeneous material were considered.

5 Engineering Characterization Of Soils

The grain size analysis result revealed that the dominant soil types found in the study area are identified as fine-grained soils (Silty-clay soils). Similarly, the atterberg (liquid limit) test analysis result revealed that the soils in the area contains an average liquid limit of more than 50% and have a plasticity index ranging from 17.18–44% (Table 13) and classified as high plasticity soils (Ramana 1993). Moreover, natural moisture content and the specific gravity of the soils range from 25.18–41.96% and 2.54 to 3.3 respectively. According to USCS, the soil samples from the reservoir area fall in MH/OH and CH/OH region which implies clayey-silty soil and silty clay soil respectively (Table 12).

Table 12
Grain size distribution, atterberg limit analysis and USCS result

Location of Test Pit	Test Pit No		Grain Size Distribution, %				Atterberg Limits, %			USCS	Plasticity Class (Ramana, 1993)
			Gravel	Sand	Silt	Clay	LL	PL	PI		
Reservoir area(Left river bank)	LTP1		0	21	42	37	70.02	35.55	34.47	MH or OH	High Plasticity
	LTP2	LTP2a	0	17	38	45	85.87	41.87	44.00	MH or OH	High Plasticity
		LTP2b					84.07	46.13	37.94		
	ATB TP 3		0	5	95		63	38	25	MH/OH	Medium Plasticity
	CHB TP 5			5.7	94.25		56	36	20	MH/OH	Medium Plasticity
Reservoir area(Right river bank)	RTP2	RTP2a	0	11	34	55	57.37	39.47	17.90	MH or OH	High Plasticity
		RTP2b					77.40	45.99	31.41		
	RTP3		0	9	38	53	63.20	39.41	23.79	MH/OH	Medium Plasticity
	SDI TP1		0	5.84	38.1	56.06	54.48	31.32	23.16	MH/OH	Medium Plasticity
	SDI TP2		0	4.39	33.6	62	56.7	29.14	27.56	CH/OH	Medium Plasticity
	MBTP1		0	3	95.6		67	40	20	MH/OH	Medium Plasticity
	DHB TP1		0	3.5	96.5		64	41	23	MH/OH	Medium Plasticity
Downstream	RTP1	RTP1a	0	8	40	52	59.47	42.28	17.18	MH or OH	Medium Plasticity
		RTP1b					63.46	40.81	22.64		

6 Water Tightness Analysis

6.1 Permeability of Soils

The result of permeability tests in the laboratory revealed that the coefficient of the permeability of soils in the study area ranges from $2.693*10^{-7}$cm/s to $6.687*10^{-5}$cm/s (Table 13) which can be classified as impervious to semi-pervious permeability respectively (USBR 1987). It can be concluded that the permeability of the soils in the reservoir site is relatively small and watertight.

Table 13
Permeability test results

Location	Test Pit No	Depth(m)	Sample Type	Specific Gravity	Permeability(cm/s)	Classification (USBR 1987)
Reservoir area (Left river side)	LTP1	0–1.5	Disturbed sample	3.2	$1.074*10^{-6}$	Impervious
	LTP2	0–2	Disturbed sample	2.9	$2.693*10^{-7}$	Impervious
	ATB TP 3	0.20–2.10	Disturbed sample	2.54	$4.61*10^{-6}$	Semi pervious
	ATB TP 4	0.10–0.80	Disturbed sample	2.56	$2.31*10^{-6}$	Semi pervious
	ATB TP 6	0.20–2.40	Disturbed sample	2.54	$1.64*10^{-6}$	Impervious
Reservoir area (Right river side)	RTP1	0–2	Disturbed sample	2.9	$6.687*10^{-5}$	Semi pervious
	RTP2	0–2	Disturbed sample	3.3	$1.528*10^{-5}$	Semi pervious
	RTP3	0–1.75	Disturbed sample	3.3	$2.74*10^{-6}$	Impervious
	CHB TP 5	0.20–1.75	Disturbed sample	2.79	$1.59*10^{-6}$	Impervious
	DHB TP1	0.10–2.10	Disturbed sample	2.69	$3.14*10^{-6}$	Semi pervious
	MBTP1	0.20–1.40	Disturbed sample	2.70	$6.2*10^{-6}$	Semi pervious

6.2 Permeability of Rock Mass Analysis

The permeability of rock mass is mainly affected by the discontinuity characteristics such as orientation, spacing, conditions of discontinuity and the stress applied on the fractures (Berhane et al. 2013). The permeability of rock masses was estimated using Eq. 2 and packer test for surface and sub-surface rock mass respectively.

Accordingly, for surface rock mass the results showed that the hydraulic conductivity of rock mass ranges from $2.9*10^{-4}$m/s to $1.3*10^{-1}$m/s and $1.3*10^{-4}$m/s to $1.2*10^{-2}$m/s with permeability class ranging from moderate to high permeable classes at dam abutments and in the reservoir area respectively (Bell 2007) and the distribution of permeability of surface rock mass at dam abutments and in the reservoir area were shown in Fig. 11. This implies that the rock mass in the area is affected by the high degree of fracturing and weathering. Besides, in the abutments of the dam, there are widely opened joints filled by secondary fine materials particularly in the left abutment while in the right abutment some fractures are not filled and are interconnected to each other. Therefore, there will be a significant amount of water leaking through these openings and serious water losses from the reservoir will occur through the dam abutments after the water is impounded in the reservoir.

Similarly, the subsurface exploration of the Arjo Didesa dam site was conducted by drilling boreholes to determine the geotechnical properties of the subsurface rock mass. This drilling result showed that the subsurface rock mass that is found at the dam site was characterized by different degree of weathering and fracturing. However, the degree of weathering is relatively decreasing as depth increases (Fig. 12). Packer tests were conducted by Oromia Water Works Design and Supervision Enterprise in 11 drilled boreholes on the dam abutments and at the center of the river in order to

determine the permeability of subsurface rock mass. The depth of these boreholes varies from 20m to 92m. The test section interval was varied from 2.5 to 5m and it depends on the condition of the rock mass with depth. Furthermore, the permeability of a rock mass along the dam axis was interpreted and classified based on Lugeon values (Fell et al. 2005) (Fig. 15) through integration of the surface and subsurface rock mass permeability results. The packer permeability test result revealed that the average minimum and maximum Lugeon values at the left abutment, right abutment and center of river bed range from 2.45 to 54.92, 13.6 to 34.23 and 8.85 to 17.38 respectively (Table 14). This suggests that the presence of highly permeable and open joints in the rock mass which is classified as permeable rock (Fell et al. 2005). Many researchers stated that as the overburden increases with depth, the permeability of the rock mass decreases (Lee and Farmer 1993 and Berhane 2013). Similarly, the permeability of the rock mass decreases as depth increases (Figs. 13 and 15).

The flow type can be determined from the packer test and it is used to determine the characteristics of discontinuities and grouting types. Thus, at the left abutment, the laminar flow is the dominant flow type (> 40%) which is followed by the dilation flow type (> 23%) and the less dominant ones include turbulent, void filling and washout flow types(Fig. 14). The dominated laminar flow in the left abutment indicated the presence of a parallel joint opening with low lugeon values (Rozo, 1933). On the other hand, turbulent flow type was observed most frequently at the center of the river (Fig. 14) which shows the presence of either open joints with high discharge or tight joints with low discharge (Ajalloeian 2013). Similarly, in the right abutment void filling is the dominant flow type (> 28%) followed by dilation (> 21%) and washout (> 21%) and less dominant ones such as laminar (14%) and turbulent flow (14%) (Fig. 14). The void filling behavior indicated that the presence of the larger joint apertures and during the test, water is progressively filling the open discontinuities or swelling occurs in the discontinuities (Houlsby 1976).

Table 14
Lugeon test results at different boreholes in the dam site

BH ID	Easting	Northing	Depth (m)	No of Test	Lugeon Range		Average of Lugeon	Average permeability, K (cm/s)
					Min.	Max.		
AD1	243064	942314	33.3	6	0.01	30	7.065	$9.184*10^{-5}$
AD2	243102	942300	40	7	0.04	34.62	11.38	$1.48*10^{-4}$
AD7	243607	942365	29	5	1.25	4.23	2.45	$3.19*10^{-5}$
AD8	242992	942179	20	4	0.24	91.54	54.92	$7.14*10^{-4}$
AD9	243029	942329	60	10	1	141.54	41.85	$5.44*10^{-4}$
AD5	243321	942643	41.7	7	1.17	26.85	13.62	$1.77*10^{-4}$
AD6	243605	942813	30	7	0.12	9.23	14.2	$1.846*10^{-4}$
AD10	243315	942329	60	11	0	171.54	20.31	$2.64*10^{-4}$
AD11	243374	942700	20	4	0.28	117.69	34.23	$4.45*10^{-4}$
AD3	243007	942365	92	14	0	42.54	8.85	$1.15*10^{-4}$
AD4	243198	942488	50	9	0	34.69	17.38	$2.26*10^{-4}$

7 Conclusion And Recommendation

On the basis of this study, the following conclusions and recommendations can be made.

- The current study assessed the geological and geotechnical conditions of materials with respect to slope stability and water tightness along the dam abutments and reservoir area. Detailed fieldwork and laboratory analysis was conducted on representative samples to determine the index and engineering properties of the soils and rocks.
- Slope stability assessments of the dam abutments were carried out through different approaches such as the Kinematic, limit equilibrium and finite element method. Kinematic analysis revealed that at both LAS1 and RAS1 slope sections were potentially unstable due to planar mode of failures. Further stability analysis using the deterministic method revealed that both LAS1 and RAS1 slope sections were found to be unstable in saturated condition which develops pore water pressure that significantly contributed to destabilize these slope sections.
- Similarly, stability analyses of LAS2 and RAS2 slope sections were performed using FE and LE methods in different conditions. The analyses result showed that both slope sections were unstable only in saturated conditions as pore water pressure can be developed to destabilize these slope sections. The FOS calculated from FE method was slightly smaller than that was calculated by LE method. Thus, it could be concluded that the results of both FE and LE methods were in good agreement at different anticipated conditions when simple slope geometry and heterogeneous materials are considered.
- The surface discontinuity survey and packer test results revealed that permeability of the rock masses at the dam abutments range from low to high permeability classes. Thus, excessive leakage will be expected after the reservoir is impounded especially through the dam abutments through fractured rocks.
- The soil permeability tests in the study area range from impervious to semi pervious ones. Thus, the leakage path is long and the potential leakage from the reservoir is not expected after the final filling of the reservoir but during the initial reservoir filling.
- Rock bolt and anchors are recommended as remedial measures to prevent planar sliding and stabilize slopes. For LAS2 and RAS2 slope sections, the failed material should be first removed to reduce the slope angle and then shotcrete should be applied to increase the stability of the slope by providing sufficient drain holes to remove pore water pressure that is building underneath the shotcrete surface. Grouting is recommended at both abutments to prevent the leakage problems when larger open joints are present. This study strongly recommends further assessment to be done for the design and installation of different remedial measures and the effect of rapid drawdown of water on slope instability of the dam abutments.

Declarations

Acknowledgment

The author expresses his sincere thanks to Oromia Water Works Design and Supervision Enterprise for the data provision and allowing for laboratory tests. My special thanks go to Addis Ababa Science and Technology University (Geology and Civil Engineering Departments) for the provision of filed equipment and some laboratory works. In addition, Bule Hora University is also acknowledged for the financial support to the first author during his MSc study. The first author would like to extend his sincere and heartfelt thanks to his advisor, Dr. Matebie Meten, for his constructive comment, encouragement, and tireless support.

References

Abdulkadir M (2009) Assessment of Micro-Dam Irrigation Projects and Runoff Predictions for Un-gauged Catchments in Northern Ethiopia, Ph.D. Dissertation, Muenster University, Germany.

Ajalloeian R and Azimian A (2013) Geotechnical Engineering Assessment of the Nargesi. 1369–1392. https://doi.org/10.1007/s10706-013-9661-3.

Alistair A and Gebremedhin T (2003) Geological setting and tectonic subdivision of the Neoproterozoic orogenic belt of Tulu-Dimtu, Western Ethiopia. Journal of African Earth Sciences V 36 329-343.

Asfaw L M (1986) Catalogue of Ethiopian earthquakes, earthquake parameters, strain release, and seismic risk. In Proc. SAREC-ESTC Conference on Research Development and Current Research Activities in Ethiopia (pp. 252-279).

ASTM (2001) Standard test method for determination of rock hardness by rebound hammer method. ASTM Stand. 04.09 (D 5873-00).

Aydin Adnan (2009) ISRM Suggested method for determination of the Schmidt hammer rebound hardness: Revised version. International Journal of Rock Mechanics and Mining Sciences, 46(3), 627–634. https://doi.org/10.1016/j.ijrmms.2008.01.020

Barton N R (1973) Review of a new shear strength criterion for rock joints. Eng Geol. 7, 287-332.

Barton N R and Choubey V (1977) The shear strength of rock joints in theory and practice. Rock Mech. 10(1-2), 1-54.

Basahel H and Mitri H (2018) Application of rock mass classification systems to rock slope stability assessment : A case study Journal of Rock Mechanics and Geotechnical Engineering Application of rock mass classification systems to rock slope stability assessment : A case study. Journal of Rock Mechanics and Geotechnical Engineering, 9(6), 993–1009. https://doi.org/10.1016/j.jrmge.2017.07.007.

Bell F (2007) Engineering Geology, (2nd ed.) Butterworth-Heinemann (Elsevier) Burlington, MA. pp.581.

Berhane G, Martens K, Al N, and Walraevens K (2013) Journal of African Earth Sciences Water leakage investigation of micro-dam reservoirs in Mesozoic sedimentary sequences in Northern Ethiopia. Journal of African Earth Sciences,79, 98–110. https://doi.org/10.1016/j.jafrearsci.2012.10.004

Bieniawski Z T (1989) Engineering rock mass classifications: a complete manual for engineers and geologists in mining, civil, and petroleum engineering. In Engineering rock mass classifications: a complete manual for engineers and geologists in mining, civil, and petroleum engineering.

Broch E and Franklin J A (1972) The point-load strength test. International Journal of Rock Mechanics and Mining Sciences And, 9(6), 669–676. https://doi.org/10.1016/0148-9062(72)90030-7

Carranza-Torres, C., & Corkum, Brent, E. Hoek. (2002). Hoek-brown failure criterion – 2002 edition.

Cheng Y M, Lansivaara T, and Wei W B (2007) Two-dimensional slope stability analysis by limit equilibrium and strength reduction methods; Comput. Geotech. 34 137–150.

Deere D U (1968) Geological consideration. In: Stagg KG, Zienkiewicz OC (eds) Rock Mechanics in Engineering Practice, Wiley, London.

Fell R, MacGregor P, Stapledon D, and Bell G (2005) Geotechnical Engineering of Dams. In Geotechnical Engineering of Dams. https://doi.org/10.1201/noe0415364409.

Genevois R, Ghirotti M (2005) The 1963 Vaiont landslide. Giornale Di Geologia Applicata, 1: 41-52.

Gercek H Ã (2007) Poisson's ratio values for rocks. 44, 1–13. https://doi.org/10.1016/j.ijrmms.2006.04.011

Gischig V, Amann F, Moore J R, Loew S, Eisenbeiss H, and Stempfhuber W (2011) Composite rock slope kinematics at the current Randa instability, Switzerland, based on remote sensing and numerical modeling. Engineering Geology, 118(1–2), 37–53. https://doi.org/10.1016/j.enggeo.2010.11.006

Griffiths D V and Lane P A (1999) Slope stability analysis by finite elements. Geotechnique, v .49(3), pp.387-403.

Griffiths DV, Marquez RM (2007) Three-dimensional slope stability analysis by elastoplastic finite elements. Ge´otechnique 57(6):537–546

Haregeweyn N, Poesen J, Nyssen J, De Wit J, Haile M, Govers G, Deckers S, (2006) Reservoirs in Tigray (northern Ethiopia): characteristics and sediment deposition problems. Land Degradation and Development 17: 211 –230.

Hoek E, and Diederichs M S (2006) Empirical estimation of rock mass modulus. International Journal of Rock Mechanics and Mining Sciences, 43(2), 203–215. https://doi.org/10.1016/j.ijrmms.2005.06.005

Houlsby AC (1976) Routine interpretation of the Lugeon water test. Q J Eng Geol 9:303–313

Hussain G, Singh Y, Bhat G M, Sharma S, Sangra R, and Singh A (2019) Geotechnical Characterisation and Finite Element Analysis of Two Landslides Geotechnical Characterisation and Finite Element Analysis of Two Landslides along the National Highway 1-A (Ladakh Region, Jammu, and Kashmir). July. https://doi.org/10.1007/s12594-019-1272-z

ISRM (1981) Suggested methods for determining the hardness and abrasiveness of rocks. In: Brown ET editor. Rock characterization, testing, and monitoring: ISRM suggested Methods. Oxford: Pergamon: 95–6.

Johnson R B and Degraff J V (1991) Principles of Engineering Geology, John Wiley and Sons, New York, 497 pp.

Kanungo D P, Pain A and Sharma S (2013) Finite element modeling approach to assess the stability of debris and rock slopes: a case study from the Indian Himalayas. Natural hazards, v .69(1), pp.1-24.

Lee CH, Farmer I (1993) Fluid flow in discontinuous rocks. Chapman & Hall, New York.

Louis C (1974) Introduction a l'hydraulique des roches. Bull BRGM, sect III, 4:283-356.

Macfarlane DF (2009) Observations and predictions of the behavior of large, slow-moving landslides in schist, Clyde Dam reservoir, New Zealand. Engineering Geology 109(1): 5-15.

Mahboubi A, Aminpour M, and Noorzad A (2008) *Conventional and Advanced Numerical* Methods of Rock Slope Stability Analysis, A Comparison Study, Gotvand Dam Right Abutment (Iran) Case Study. 1–6.

Marinos P and Hoek E (2000) GSI a geologically friendly tool for rock mass strength estimation. Proc. GeoEng2000 Conference, Melbourne.

Memon Y (2018) A Comparison Between Limit Equilibrium and Finite Element Methods for Slope Stability Analysis. December, 0–17. https://doi.org/10.13140/RG.2.2.16932.53124

Merla G, Abbate E, Canuti P, Sagu M and Tacconi P (1973) Geological map of Ethiopia and Somalia. Explanatory notes (1979). Consiglio Nazionale Delle Ricerche, Firenze, Italy.

Mozafari M, Raeisi E, Zare M (2011). Water leakage paths in the Doosti Dam, Turkmenistan, and Iran. Environ Earth Sci. doi:10.1007/s12665-011-1069-x.

Palmstrom A (1982) The Volumetric Joint Count –A Useful and Simple Masure of the Degree of Jointing, IVth Int. Congress IAEG, New Delhi, pp.v221-v228.

Park H, and West T R (2001) Development of a probabilistic approach for rock wedge failure. *Engineering Geology*, *59*(3–4), 233–251. https://doi.org/10.1016/S0013-7952(00)00076-4.

Pain, A., Kanungo, D. P., & Sarkar, S. (2014). Rock slope stability assessment using finite element based modeling - examples from the Indian Himalayas. Geomechanics and Geoengineering, 9(3), 215–230. https://doi.org/10.1080/17486025.2014.883465

Panizzo A, De Girolamo P, Di Risio M, et al. (2005) Great landslide events in Italian artificial reservoirs. Natural Hazards and Earth System Science 5(5): 733-740.

Phase2 v8.0 User's manual available from https://www.rocscience.com/help/phase2/webhelp9/phase2.htm

Raghuvanshi T K (2017) Journal of King Saud University – Science Plane failure in rock slopes – A review on stability analysis techniques. Journal of King Saud University - Science. https://doi.org/10.1016/j.jksus.2017.06.004

Ramana KV (1993) Humid tropical expansive soils of Trinidad: their geotechnical properties and areal distribution. Eng Geol 34:27–44

Rocscience RocLab – Program (2002) For determining rock mass strength parameters using the Hoek-Brown failure criterion, Rocscience Inc., Toronto.

Rocscience (2004) Dips 6.0, http://www.rocscience.com/software/dips

Rocscience (2004) Rocdata 3.0, http://www.rocscience.com/software/rocdata

Rocscience (2004) Slide 6.0, http://www.rocscience.com/software/slide

Rocscience (2004) RocPlane 2.0, http://www.rocscience.com/software/rocplane

Rozo (1933) Lugeon Test Interpretation, Revisited. 405–414.

Shaz A, Chala E T, and Rao K S (2019) Rock Mass Slope Stability Analysis Under Static and Dynamic Conditions in Mumbai, India. Springer Singapore. https://doi.org/10.1007/978-981-13-0562-7

Snow DT (1965) A parallel plate model of fractured permeable media. Ph.D. Thesis, University of California, Berkeley.

Tefera M, Tadiwos C, Workineh H (1996) Explanation of the geological map of Ethiopia, scale 1:2,000,000. Ethiopian Institute of Geological Surveys Bull. No. 3

USBR (1987) Design of Small Dams. United States Department of the Interior, Bureau 145 of Reclamation, Denver

Vinod B R, P Shivananda, Swathivarma R, and Bhaskar M B (2017) Some of Limit Equilibrium Method and Finite Element Method based Software are used in Slope Stability Analysis, International Journal of Application or Innovation in Engineering & Management, Vol. 6, Issue 9.

Wang FW, Zhang YM, Huo ZT, et al (2004) The July 14, 2003 Qianjiangping landslide, Three Gorges Reservoir, China. Landslides 1(2): 157-162. DOI: 10.1007/s10346-004-0020-6.

Wyllie D C, and Norrish N (1996) Landslides: Investigation and Mitigation (pp. 474-504). Transportation Research Board.

Figures

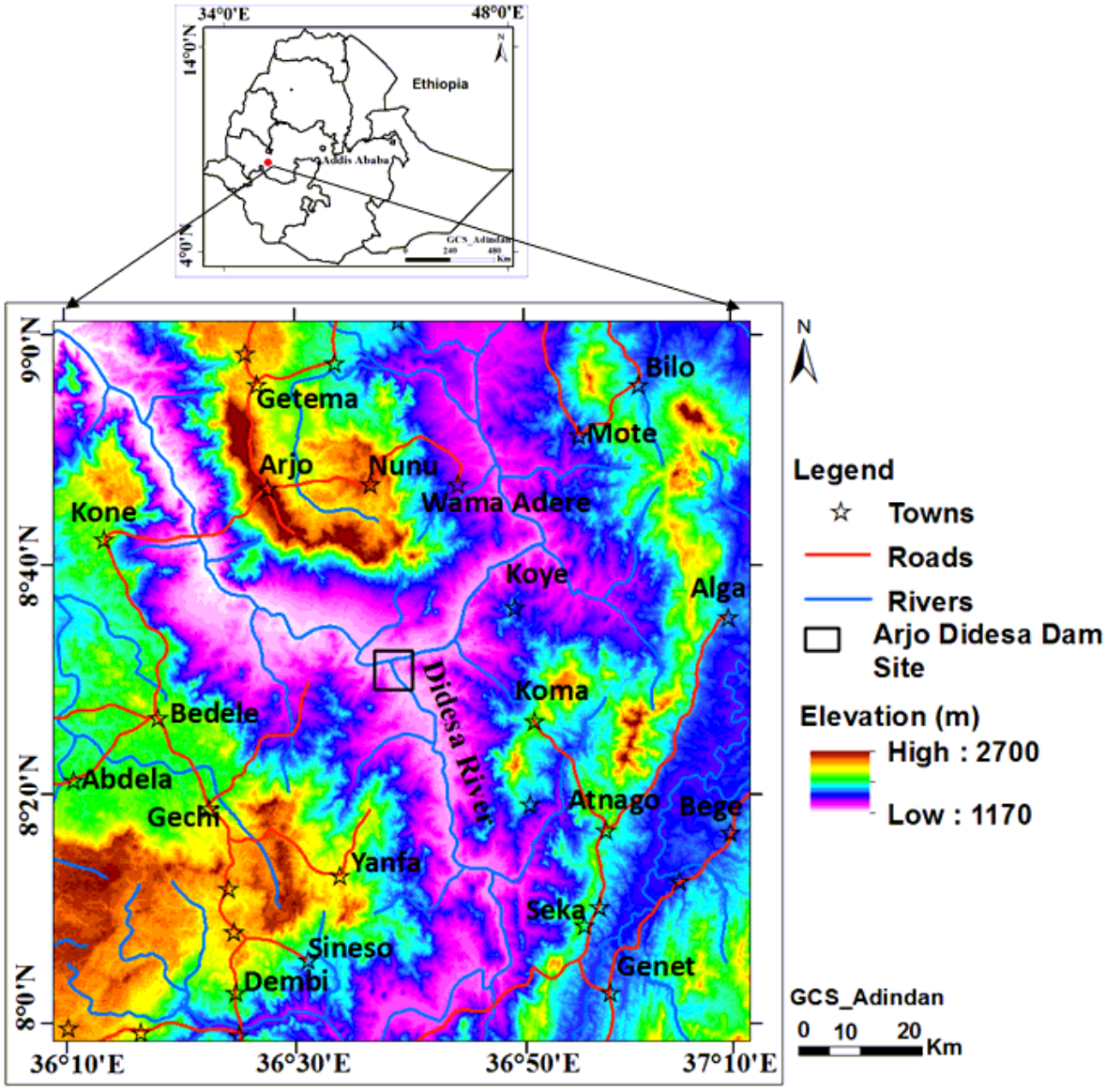

Figure 1

Location and accessibility of the Arjo Didesa dam site

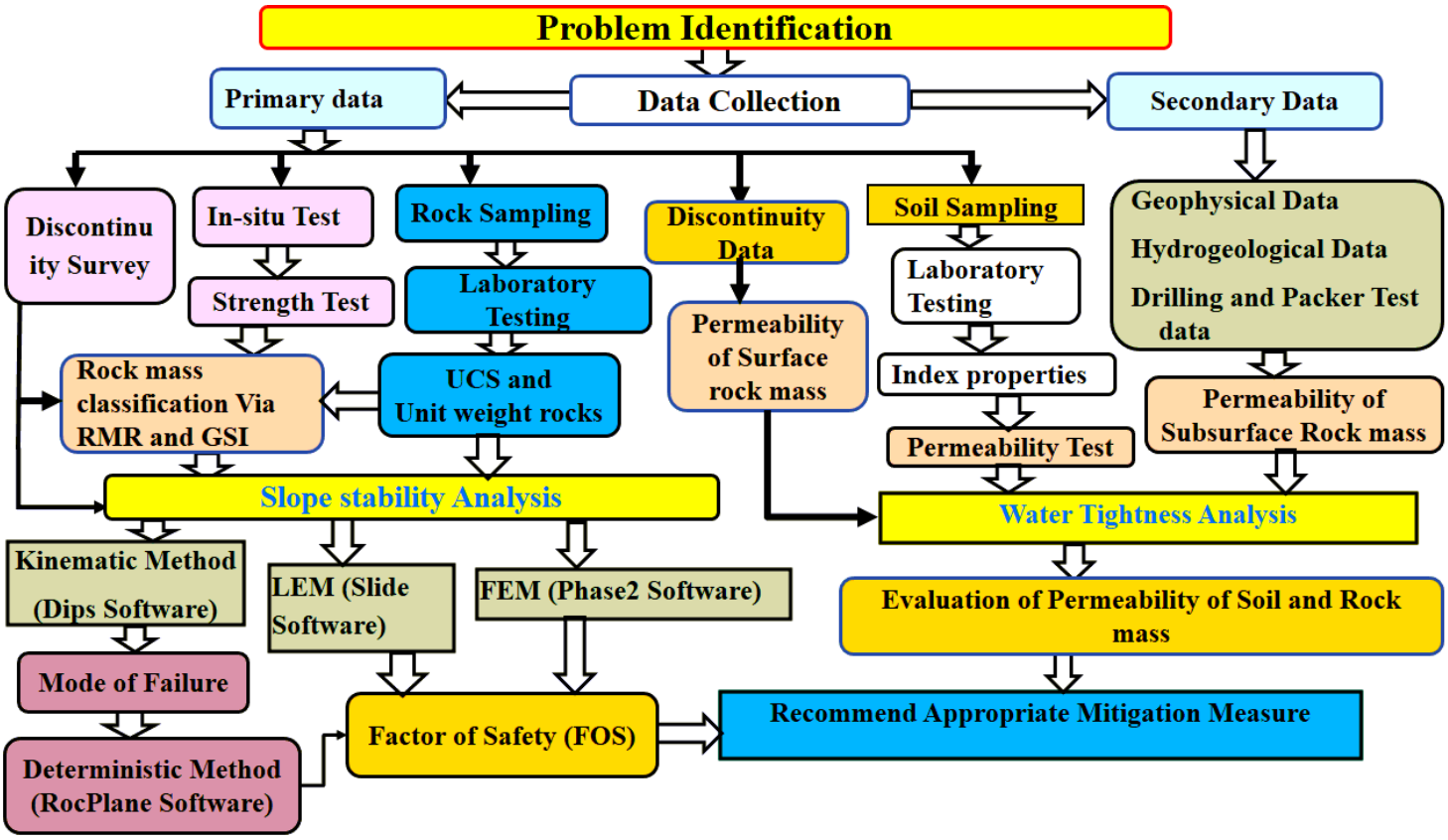

Figure 2

Flowchart showing a methodological framework of the study

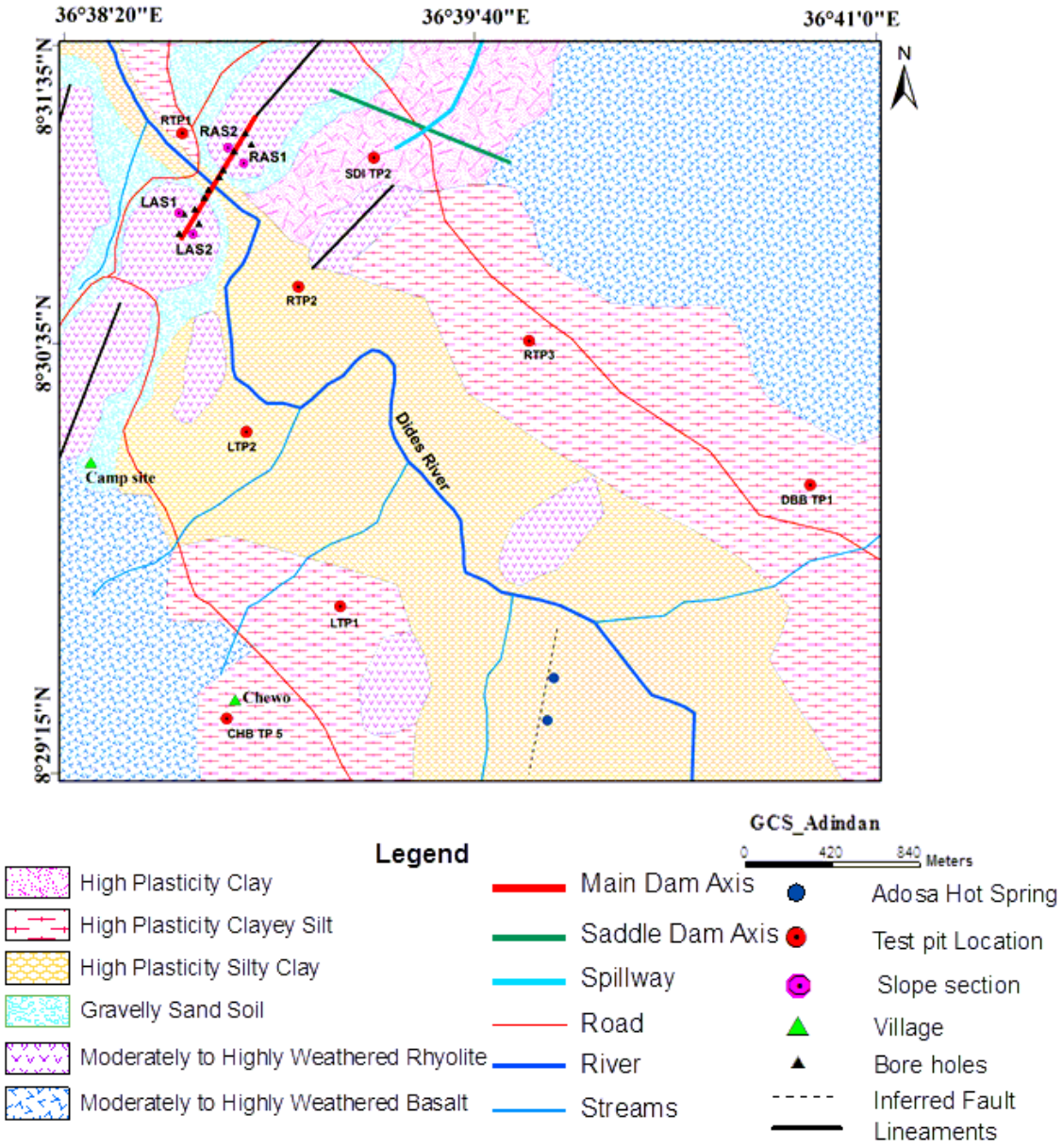

Figure 3

Engineering geological map of the study area

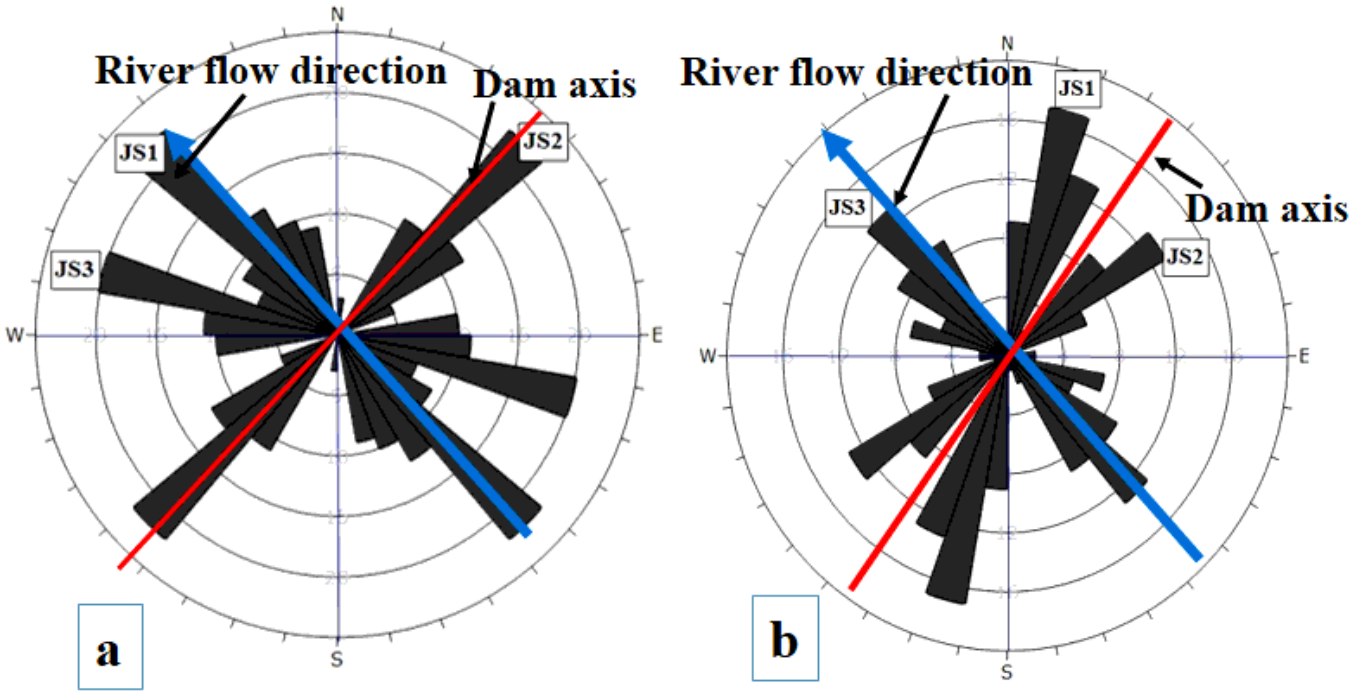

Figure 4

Rosette diagram of discontinuity strikes plotted using Dips software for A) the left abutment B) the right abutment

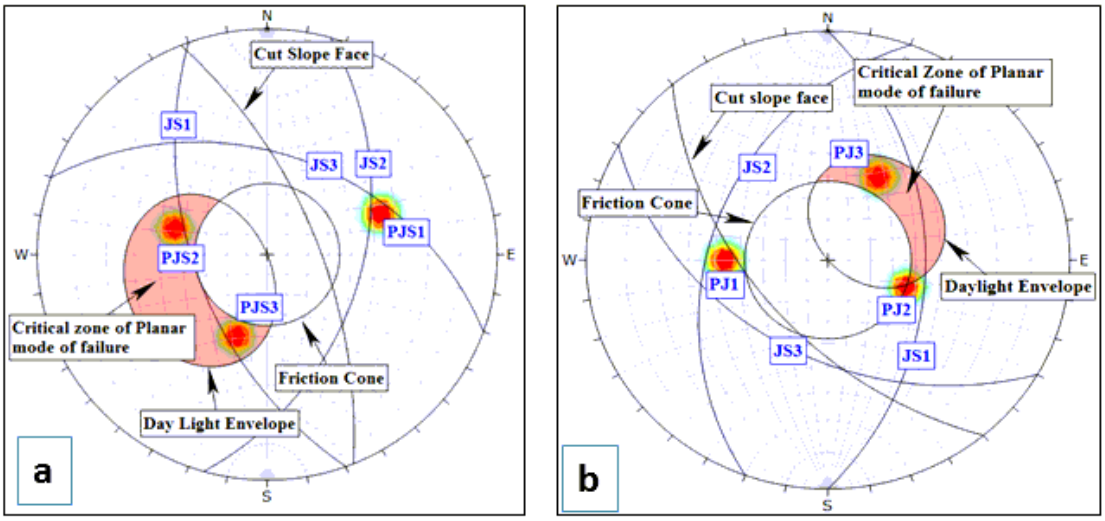

Figure 5

Kinematic analyses for planar mode of failures on (a) left abutment at LAS1 slope section and (b) right abutment at RAS1 slope section

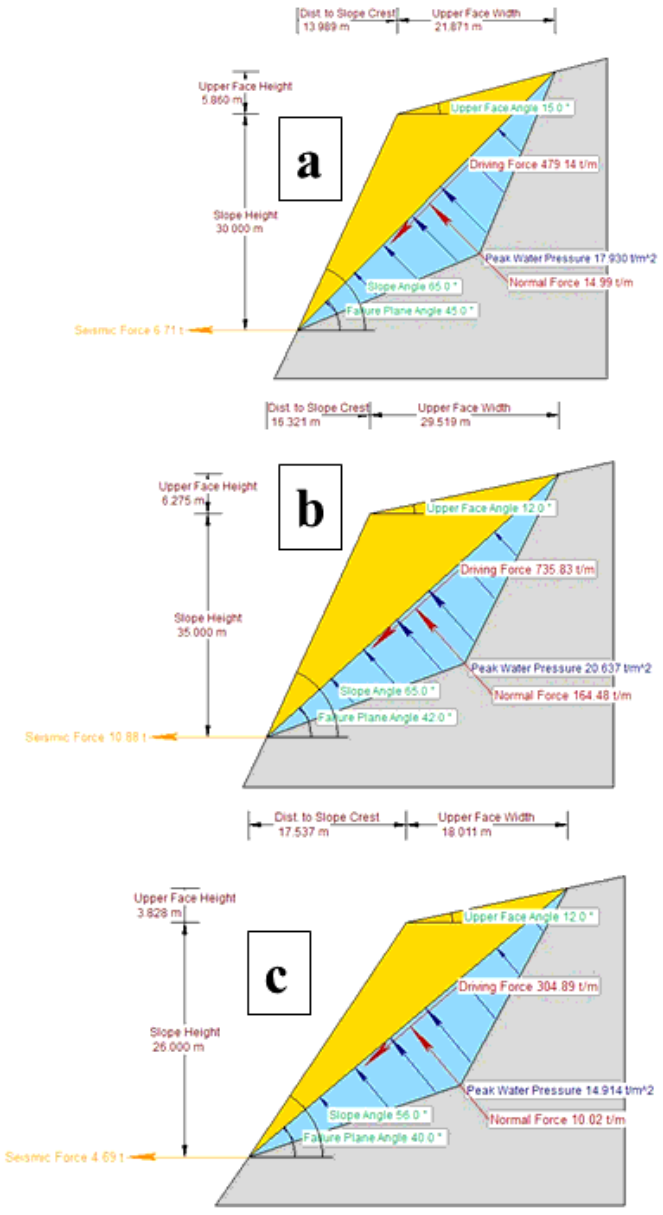

Factor of Safety	0.24
Driving Force	479.14t/m
Resisting Force	114.19t/m
Wedge Weight	670.90t/m
Wedge Volume	287.08m^3/m
Shear Strength	112.08t/m^2
Normal Force	14.99t/m
Seismic Force	6.71t
Plane Waviness	8.0°
Water Force on Failure Plane	454.66t/m

Factor of Safety	0.33
Driving Force	735.83t/m
Resisting Force	239.94t/m
Wedge Weight	1087.60t/m
Wedge Volume	465.38m^3/m
Shear Strength	228.44t/m^2
Normal Force	164.48t/m
Seismic Force	10.88t
Plane Waviness	4.0°
Water Force on Failure Plane	636.49t/m

Factor of Safety	0.32
Driving Force	304.89t/m
Resisting Force	96.83t/m
Wedge Weight	468.73t/m
Wedge Volume	200.57m^3/m
Shear Strength	95.96t/m^2
Normal Force	10.02t/m
Seismic Force	4.69t
Plane Waviness	5.0°
Water Force on Failure Plane	346.04t/m

Figure 6

Slope stability analyses results at LAS1 slope section for J2 (a) and for J3 (b) and c) for J3 at RAS1 slope section

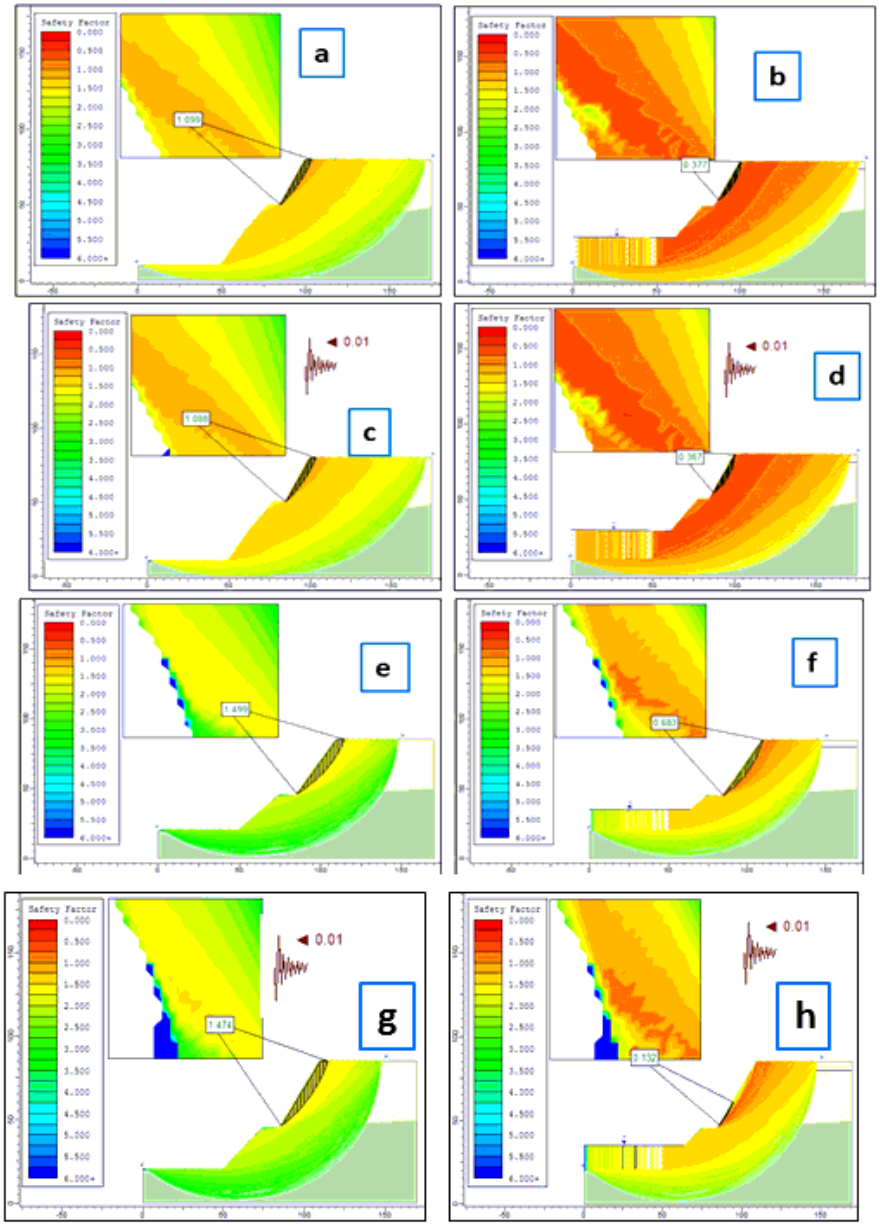

Figure 7

Slope stability analysis results using LEM at LAS2 (a, b, c and d) under static dry, static saturated, dynamic dry and dynamic saturated conditions respectively, and at RAS2 (e, f, g and h) under static dry, static saturated, dynamic dry and dynamic saturated conditions respectively.

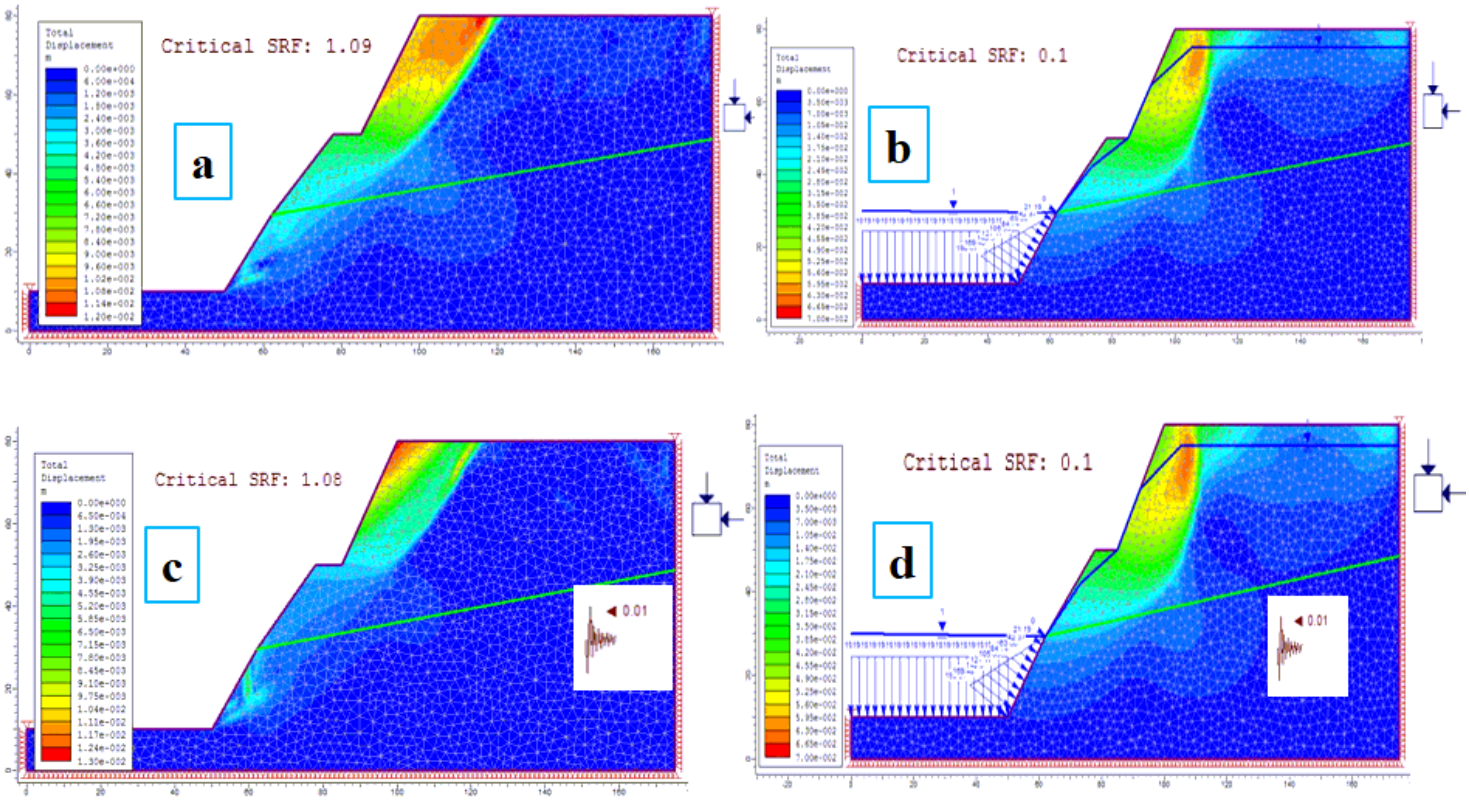

Figure 8

Slope stability analysis results using FEM at LAS2 under A) static dry condition, B) static saturated condition, C) dynamic dry condition and D) dynamic saturated condition

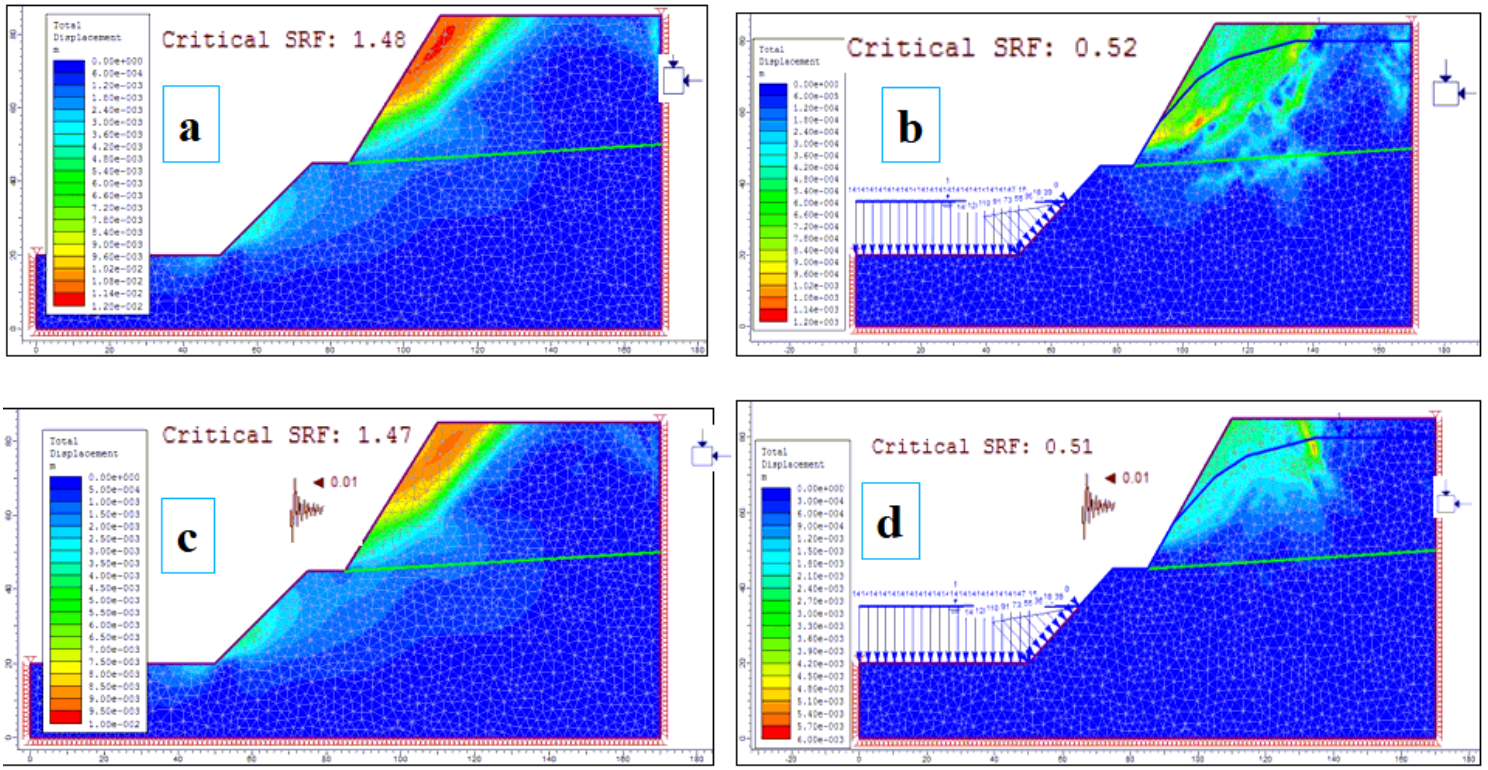

Figure 9

Slope stability analysis results using the Phase2 software for RAS2 under A) static dry condition, B) static saturated condition, C) dynamic dry condition and D) dynamic saturated condition

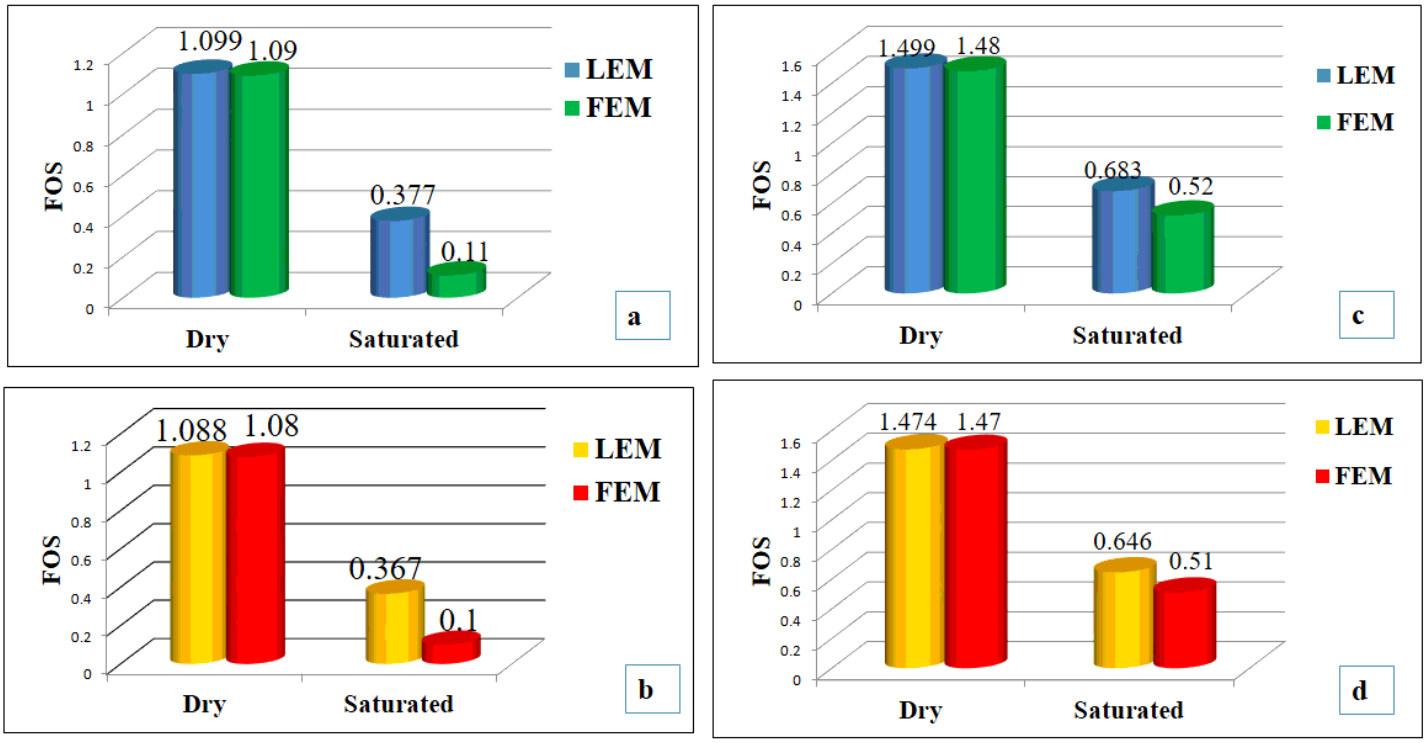

Figure 10

Comparisons of Factor of safety (FOS) determined by Phase 2 and slide Software under different anticipated conditions at LAS2 (A and B) under static and dynamic conditions respectively, and at RAS2 (C and D) under static and dynamic saturated conditions respectively

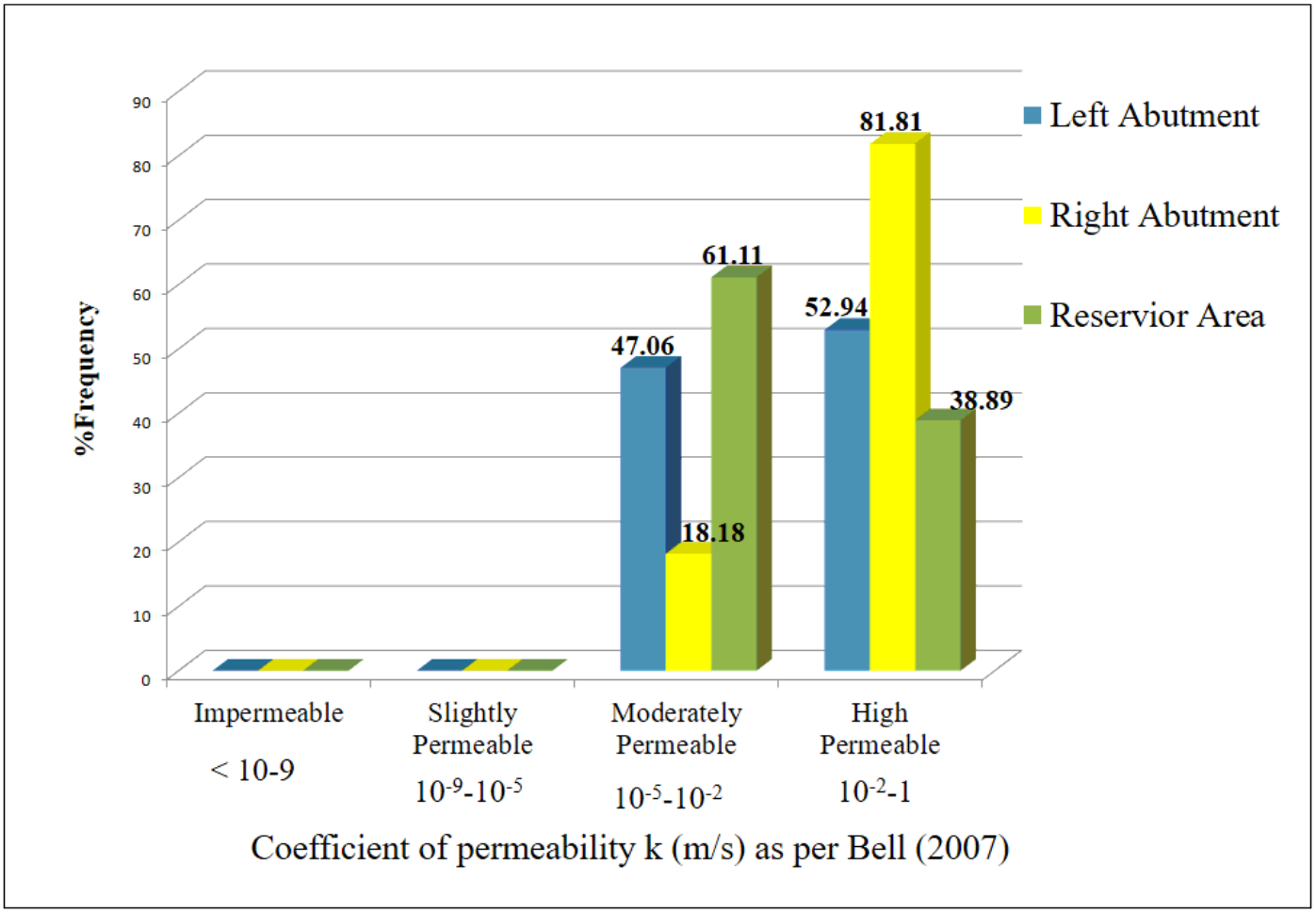

Figure 11

Percentage distribution of hydraulic conductivity of surface rock masses in the study area

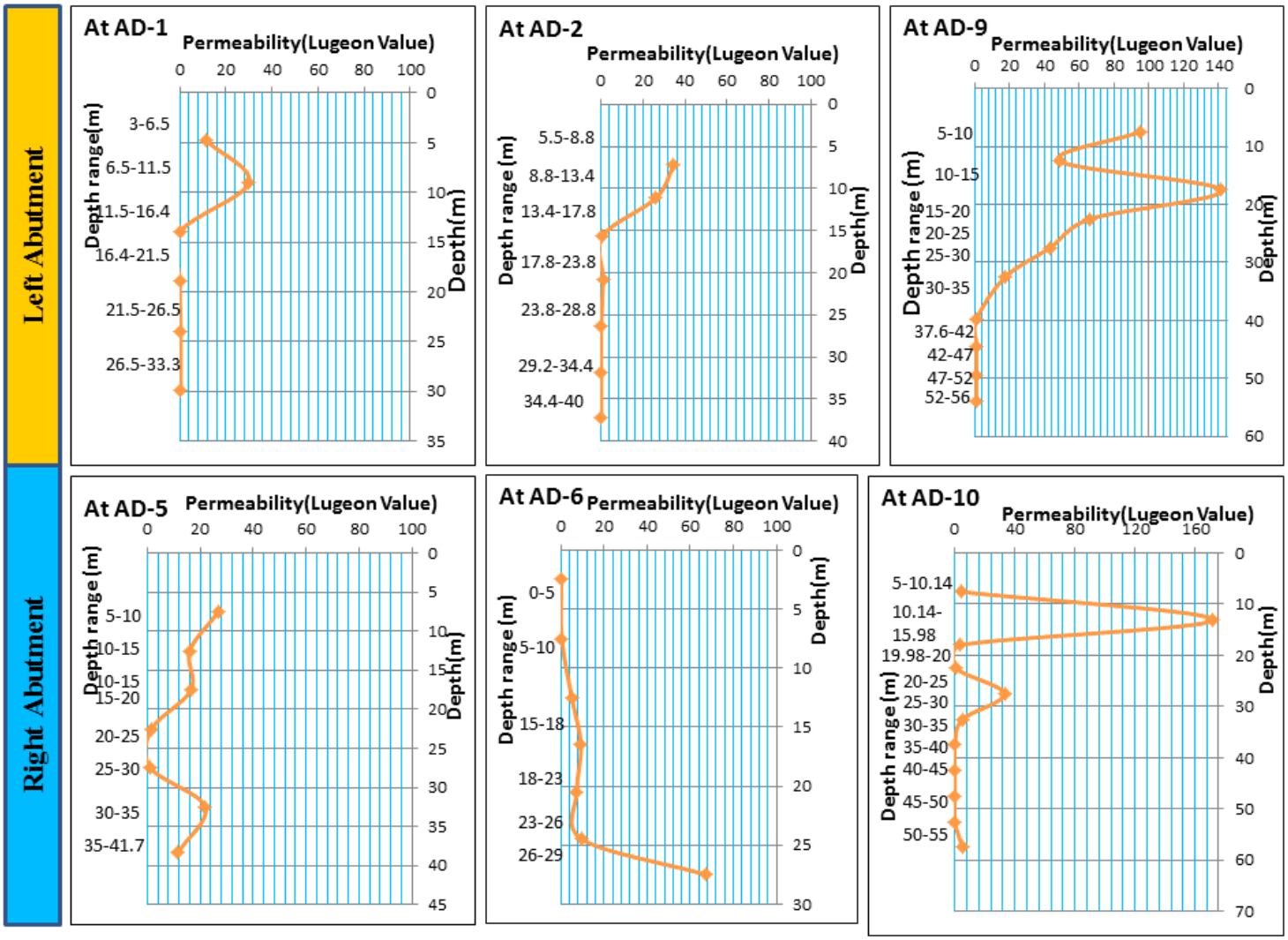

Figure 13

Variations of Lugeon values with depth for selected boreholes from the left and right abutment

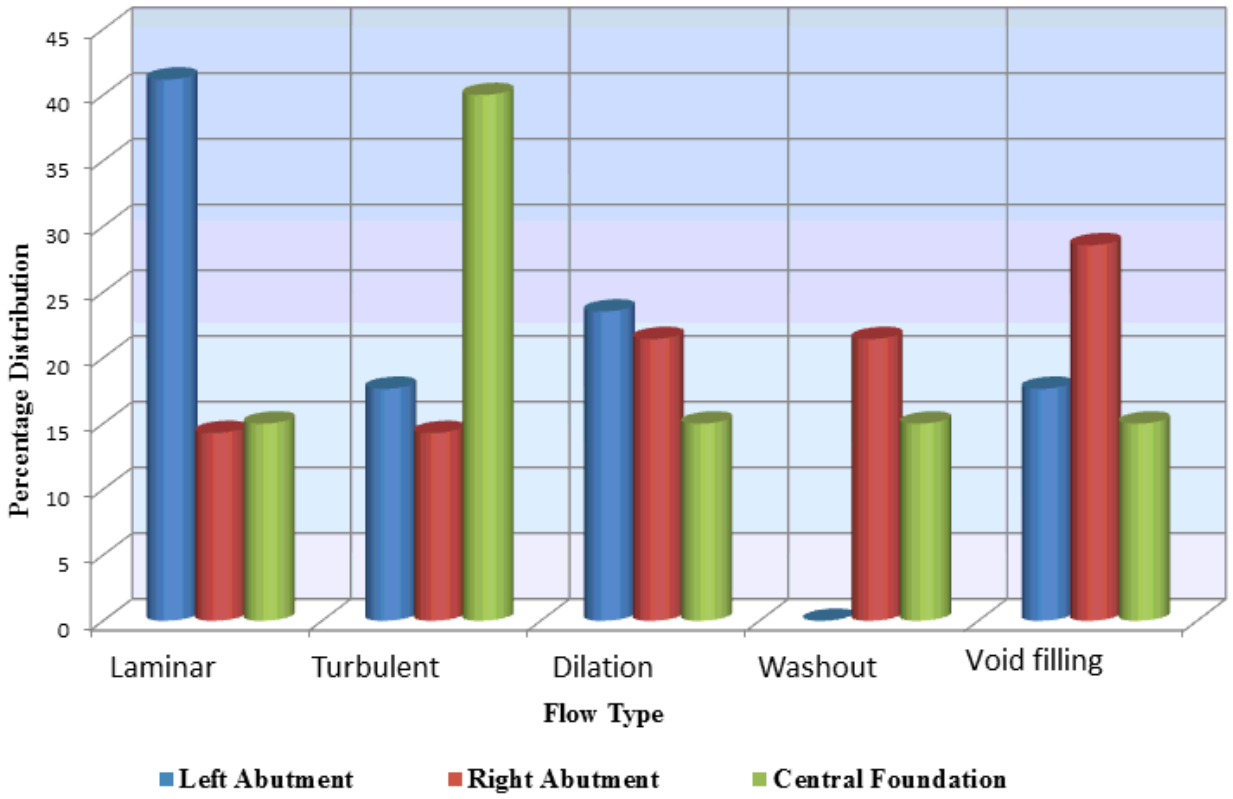

Figure 14

Percentage distribution of flow types in different boreholes

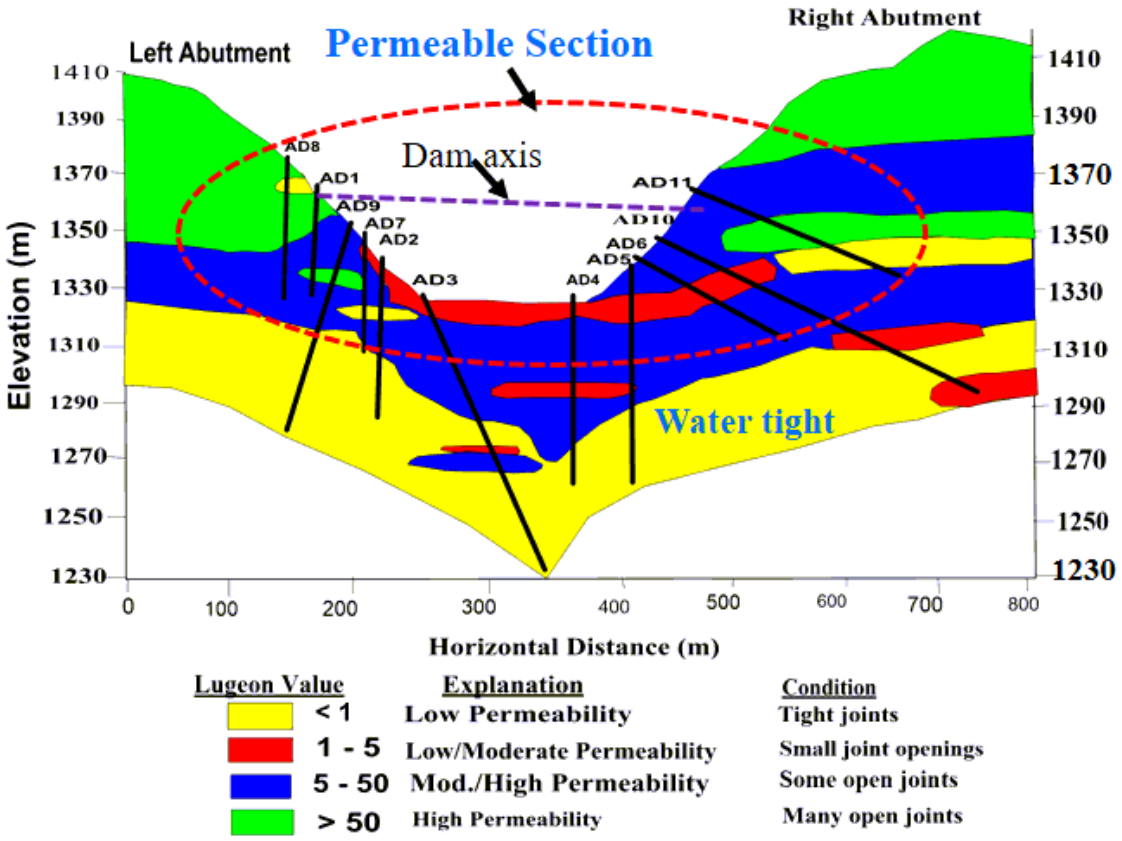

Figure 15

Permeability of rock masses along the Dam axis